



Source apportionment of black carbon and combustion-related CO₂ for the determination of source-specific emission factors

Balint Alföldy¹, Asta Gregorič^{1,2}, Matic Ivančič¹, Irena Ježek¹, Martin Rigler¹

¹Aerosol d.o.o, Ljubljana, SI-1000, Slovenia

5 ²Center for Atmospheric Research, University of Nova Gorica, Vipavska 13, Nova Gorica, SI-5000, Slovenia

Correspondence to: Balint Alföldy (balint.alfoldy@aerosol.eu)

Abstract. Black carbon aerosol (BC) typically has two major sources in the urban environment; traffic, and domestic biomass burning which has a significant contribution to urban air pollution during the heating season. Traffic emissions have been widely studied by both laboratory experiments (individual vehicle emission) and real-world measurement campaigns (fleet emission). However, emission information from biomass burning is limited, especially an insufficiency of experimental results from real-world studies. In this work, the black carbon burden in the urban atmosphere was apportioned to fossil fuel (FF) and biomass burning (BB) related components using the Aethalometer source apportionment model. Applying the BC source apportionment information, the combustion-related CO₂ was apportioned by multi-linear regression analysis, supposing that both CO₂ components should be correlated with their corresponding BC component. The combination of the Aethalometer model with the multi-linear regression analysis (AM-MLR) provided the source-specific emission ratios (ER) as the slope of the corresponding BC-CO₂ regression. Based on the ER values, the source-specific emission factors (EFs) were determined using the carbon content of the corresponding fuel. The analysis has been carried out on a three-month long BC and CO₂ dataset collected at three monitoring locations in Ljubljana, Slovenia, between December 2019 and March 2020. The measured mean site-specific concentration values were in the 3500-4800 ng m⁻³ and 458-472 ppm range for BC and CO₂, respectively. The determined average EFs for BC were 0.39 and 0.16 g/(kg fuel) for traffic and biomass burning, respectively. It was also concluded that the traffic-related BC component dominates the black carbon concentration (55-65% depending on the location), while heating has the major share in the combustion-related CO₂ (53-62% depending on the location). The method gave essential information on the source-specific emission factors of BC and CO₂, enabling better characterization of urban anthropogenic emissions and the respective measures that may change the anthropogenic emission fingerprint.

25 1 Introduction

Biomass burning (BB) is a significant source of black carbon (BC), brown carbon (BrC) and organic particulate matter, creating a contribution to climate change (Myhre et al., 2013; Tomlin, 2021) and a severe risk to human health (Naehrer et al., 2005; Janssen et al., 2011; Sigsgaard et al., 2015; Chen et al., 2017; Brown et al., 2020; Karanasiou et al., 2021). Global hotspots of BB are associated with extensive and persistent wildfires (e.g. deliberate forest burning in Amazonia and Indonesia, accidental



30 forest and savanna fires in central Africa, North America, the Mediterranean basin and Siberia) (see e.g. Val Martin et al., 2006; Giglio et al., 2013; Smirnov et al., 2015; Chiloane et al., 2017; Healy et al., 2019; Reddington et al., 2019). On the other hand, emission from domestic wood combustion for the purpose of space heating, water boiling or cooking significantly contributes to the BB emission as well, especially in locations of high population density and reduced ventilation (Karagulian et al., 2015; Klimont et al., 2017; Mitchell et al., 2017).

35 Wood combustion is an important energy source even in well-developed countries, where its emissions add to traffic-related air pollution. The emission characteristics of BB differ from that of internal combustion engines, where the combustion is more complete. Consequently, engines emit less CO, particulate matter and organic compounds per unit of fuel mass, while having higher NO_x emissions compared to BB due to the higher combustion temperature and excess of air (see EEA 2019: 1.A.3.b. versus 1.A.4.a-b.).

40 Black carbon is a dominant form of particulate matter emitted from fossil fuel (FF) combustion. Diesel engines (before the Euro 5 legislation standard) emit more than 80% of the particle mass (PM) as BC (EEA 2019: 1.A.3.b.). Since diesel vehicles dominate the European vehicle fleet (Cooper, 2020) the high traffic-related BC emission poses significant air quality problems in cities, which is complemented by the BB emission during the heating season.

Due to its harmful health effects, BC emissions of diesel engines are studied intensively worldwide for a long time (see the original work of Hansen and Rosen, 1990). The BC emission factors have been determined by numerous studies based on laboratory chassis dynamometer tests (Alves et al., 2015; Park et al., 2020), or real-world on-road measurements using either the chasing method (Wang et al., 2012; Ježek et al., 2015; Zavala et al., 2017), or on-board tailpipe measurements by PEMS (Portable Emission Measurement System) (Zheng et al., 2015; Giechaskiel et al., 2019). These tests refer to the emission factors (EF, emitted pollutant per kg of fuel, or km) of individual vehicles, and do not reflect the emission of the entire vehicle
45 fleet. On the contrary, roadside monitoring offers the opportunity to measure a statistically significant number of vehicles. These measurements are usually carried out in tunnels (Sánchez-Ccoyllo, 2005; Ban-Weiss et al., 2009; Brimblecombe et al., 2015; Blanco-Alegre et al., 2020), where elevated pollution concentration levels and negligible interference of other combustion sources (like wood burning) can be assured. In these studies, the EF calculation is usually based on the carbon-balance method (Brimblecombe et al., 2015), when the plume CO₂ increment is used to determine the burnt fuel mass.

55 On the contrary, emissions from biomass burning are not controlled nearly as strictly as from mobile sources. Some studies have investigated specific combustion appliances, providing the emission factors of various pollutants (Querol et al., 2016; Nielsen et al., 2017; Holder et al., 2019; Trubetskaya et al., 2021). The advantages of these studies are the controlled experimental conditions, the information about the combustion parameters (fuel type, combustion temperature, excess of air) and the opportunity to change these parameters, thus EFs concerning a wide spectrum of fuels and combustion conditions were
60 reported. However, since only a limited number of stoves and combustion scenarios were studied it is difficult to extrapolate these results to a “real-world situation” of a city.

For this reason, other papers focus on the real-world situation and report the atmospheric concentrations of the biomass burning related air pollution. However, since the contribution of the traffic emission always interferes, the pure biomass burning related



air pollution is difficult to study. Consequently, some studies selected specific locations like Glojek et al., (2021) in Loški
65 Potok, Slovenia, that can be considered as a model village of biomass burning emission with negligible contribution of other
sources of air pollution. Other studies utilise the integrated source apportionment model of the Aethalometer (Sandradewi et
al., 2008) and reported BB- and FF-related BC concentrations separately (see e.g., Dumka et al., 2018; Deng et al., 2020;
Liakakou et al., 2020; Mbengue et al., 2020; Milinkovic et al., 2021).

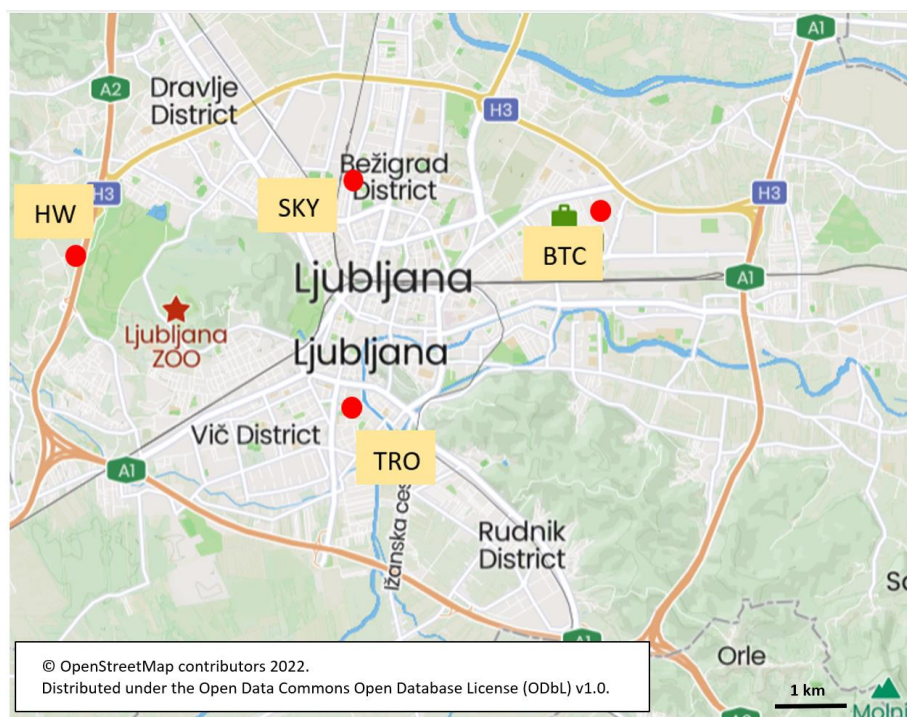
Despite the reliable source apportionment model of the Aethalometer, the adaption of the carbon-balance method from traffic
70 emission studies is problematic due to the lack of the CO₂ source apportionment. However, inverse modelling can offer an
opportunity to track the air pollution back to their sources. For example, Olivares et al. (2008) applied inverse modelling to
retrieve the traffic- and BB-related emission factors of NO_x, PM₁₀, BC, and particle number.

In this paper we aimed to determine the biomass burning and traffic specific BC emission factors in urban atmosphere during
the heating season. We used the carbon-balance method that required the simultaneous source apportionment of BC and CO₂
75 concentrations. The BC source apportionment was performed by the integrated model of the BC monitor (Aethalometer model,
AM), while the source apportionment of CO₂ was implemented by multi-linear regression analysis (MLR). After the source
apportionment of both components, the specific emission ratios (ERs) for BB and FF have been determined and converted to
EF values following the carbon-balance method. The measurements were taken during a three-months long monitoring
campaign in Ljubljana, Slovenia, during winter 2019-2020. The atmospheric concentration of black carbon was monitored
80 with simultaneous CO₂ measurement at three locations of the city with different emission characteristics involving traffic and
heating-related emissions, as well as an urban background site.

In the following we introduce our combined Aethalometer model – multi-linear regression analysis (AM-MLR) method that
we applied for the determination of the source-specific emission factors. We present the BB- and FF-related emission factors
for three different locations of the city. In order to validate the AM-MLR method, an auxiliary measurement campaign was
85 performed during summer, when only fossil fuel combustion was assumed to present. The FF-related emission factors
determined during the summer campaign was compared to the result of the AM-MLR method.



90



95 **Figure 1: Measurement locations on the map of Ljubljana. HW shows the location of the traffic measurement next to the highway.**



2 Methods

2.1 Measurement sites and instrumentation

100 The measurement campaign took place from December 2019 to March 2020. Three measurement sites were selected in the city with different microenvironments, source profiles and emission activity (Figure 1). One location was selected in the historical center of the city (Trnovo, TRO), where wood combustion represents the primary energy source for domestic heating during winter. This site is located in the restricted traffic area of the old town, where low direct vehicle emission is expected. The measurement setup was installed in a family house, with the sampling inlet on the roof, 8 m above the ground.

105 Another location was selected close to major roads and far from biomass burning sources that ensured to measure higher relative contribution of traffic emission. The instruments were installed in a waterproof cabinet in the open recreational area of the Atlantis sport complex in the BTC commercial center (BTC site). The inlet was mounted at 3 m height.

The third measurement location was the atmospheric observatory of Aerosol d.o.o (Skylab, SKY) that is considered to be an urban background location. This location is far from the major roads of the city and not affected directly either by traffic
110 emission or wood combustion. The sampling inlet was at 10 m above the ground.

The equivalent black carbon (eBC, referred as BC in the following) concentrations were monitored using multi-wavelength Aethalometers (AE33, Magee Scientific/Aerosol d.o.o. Slovenia, Drinovec et al., 2015) that measures the light attenuation of the particle sample collected on a TFE-coated glass filter tape (M8060) at seven wavelengths (370 – 950 nm). The absorption coefficient of the particle sample (b_{abs} , Mm^{-1}) was obtained by dividing the attenuation coefficient by the multiple scattering
115 parameter ($C=1.39$ for M8060 filter tape; Weingartner et al., 2003). The BC mass concentration were generated as the ratio of the absorption and the wavelength dependent Mass Absorption Cross-section parameter (MAC_{λ} , m^2g^{-1}) provided by the manufacturer. Aerosol size selection was provided at the inlet of the Aethalometer by a cyclone sampling head with $\text{PM}_{2.5}$ cut-off diameter. The flow rate was set to 5 l/min and the measurement time resolution to 1 min. The “dual spot” technology enables the real-time loading effect correction, which is especially important when spectral dependence of optical absorption
120 is used for source apportionment.

The CO_2 concentrations were measured by flow-through CO_2 sensors (Carbocap GMP 343, Vaisala, Finland). The CO_2 sensors were directly connected to the exhaust of the AE33, thus analysing the identical air stream as the Aethalometer. The accuracy of the sensor is 3 ppm below 1000 ppm concentration range, which was the case during the campaign even in the most polluted days. The response time of the sensor is comparable with the AE33, so the 1-minute average signals of BC and CO_2 were well
125 correlated when common sources were measured.

The three measurement systems were compared in the air quality laboratory of Aerosol d.o.o before the campaign. The variation between the AE33 units was below 1% at 1 minute averaging time for both wavelengths used for source apportionment (470 and 950 nm). This precision was expected from the results of Cuesta-Mosquera et al. (2021), who



130 compared 23 AE33 units and found variation between the measurement results less than 1%. The unit-to-unit variability of the
CO₂ sensors the was below 4 ‰ on 1 minute time basis.

2.2 Meteorological situation

The measurement campaign started on the 6 of December 2019, during a warming up period that was continued by an unusually
warm and dry January and February (Figure 2). Table 1 summarises the basic climatological anomalies comparing to the
reference long-term averages of the 1981-2010 period. The average monthly temperatures in Ljubljana during the three-month-
135 long campaign were warmer than the long-term averages of the 1981–2010 period (2.3 °C, 1.7 °C and 4.8 °C above the long-
term average on December, January, and February respectively). February 2020 was the second warmest February in the
history of measurements. Usually, January and February are the driest periods of the year, and in 2020, they were even drier
than the average. The snow cover was negligible, limited to few days during the measurement period.



140

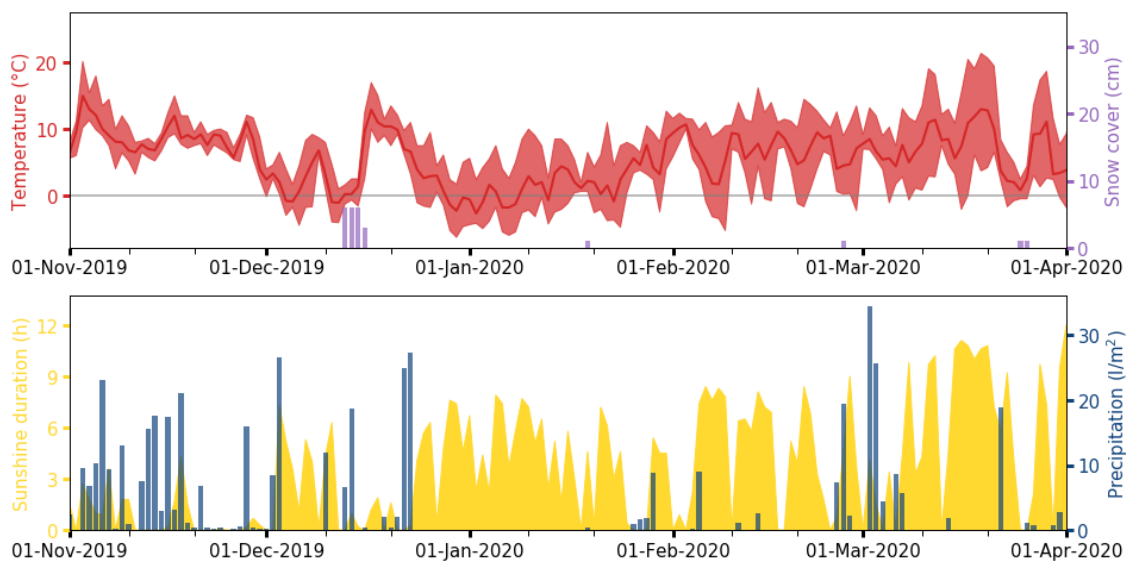


Figure 2: Time series of minimal, mean, and maximal daily temperatures, snow cover, daily sunshine duration and daily precipitation accumulation in Ljubljana from November 2019 to March 2020.

145



Table 1: Monthly meteorological anomalies relative to reference long-term averages of the 1981–2010 period.

Anomaly	2019		2020		
	November	December	January	February	March
Temperature	+ 3.1 °C	+ 2.3 °C	+ 1.7 °C	+ 4.8 °C	+ 0.7 °C
Precipitation	146%	121%	20%	60%	119%
Sunshine duration	39%	156%	186%	121%	119%



150 2.3 Emission Ratio (ER) and Emission Factor (EF) calculation

Air pollution emission from combustion sources is usually reported with respect to burnt fuel mass and given in fuel consumption-specific emission factor (EF) in $\text{g}(\text{kg fuel})^{-1}$ units. Although the combustion is never complete, more than 99% of the fuel carbon content is oxidized to carbon dioxide (EEA, 2019) that can be used as a tracer for fuel consumption estimation. Dividing the pollution concentration by the CO_2 increment of the plume, the pollution-to- CO_2 emission ratio (ER) can be determined.

The concentration ratio of two particular components of the plume can be calculated by an integrative or derivative way. If the time resolution of the measurement technique of the two components differs significantly, the two concentrations would not be correlated even if they have a common source. In this case, the integrative method is the preferable option for ER calculation. This way the time integral of the concentration peaks are calculated (peak area), and the ratio of the net peak areas (after background removal) provides the ER (see e.g. Ježek et al., 2015). The disadvantage of this method is that the peak identification is arbitrary, and the background definition and removal burden the calculation by an additional uncertainty.

On the other hand, if the time resolution of the two measurement techniques is similar, the recorded pollutant concentrations originated from a common source are correlated in time. In this case a threshold value can be defined for the minimum required R^2 of the correlation. Above the threshold R^2 the two components are considered to originate from the same source and the slope of regression provides the ER (derivative way). The offset of the regression line depends on the background concentrations that does not need to take into consideration during the calculation.

In our case the BC/CO_2 ER was calculated by the derivative method, and later it was transformed to EF using the carbon content of the concerned fuel:

$$170 \quad EF [\text{g}(\text{kg fuel})^{-1}] = ER(\mu\text{g m}^{-3}/\text{ppm}) \cdot \frac{1}{1.82} \cdot \frac{44}{12} \cdot CC, \quad (1)$$

where CC is the carbon content of the fuel that is 0.86 for diesel oil and petrol (Huss et al., 2013), while 0.45 for dry wood (pine tree – Goncalves et al., 2012). The measured CO_2 concentration was converted from ppm to mg m^{-3} using $1.82 \text{ mg m}^{-3}/\text{ppm}$ conversion factor considering the AMCA atmospheric standard ($T=21 \text{ }^\circ\text{C}$, $P=1 \text{ bar}$) that was also applied by the Aethalometer for the BC concentration calculation. Molecular weight of CO_2 (44) and C (12) was used to calculate the carbon mass fraction in CO_2 .

2.4 Source apportionment and source-specific emission ratios

Measurement of the spectrally resolved absorption coefficient provides an insight into the composition of light absorbing particles, allowing to distinguish the highly (and widely) absorbing black carbon (soot) particles from brown carbon (light-absorbing organic aerosols) (Bond & Bergstorm, 2006; Drinovec et al., 2015). Fossil fuel combustion generates mostly pure soot particles that are strong light absorbers over the whole NIR-visible wavelength domain, while particles generated by



biomass burning contain other light absorbing compounds such as brown carbon that have characteristic absorbance bands in the near UV domain (Sandradewi et al., 2008; Helin et al., 2018).

185 Sandradewi et al. (2008) developed the so called ‘Aethalometer model’ where the absorptions at 470 and 950 nm wavelengths were expressed as the sum of the absorptions of the FF- and BB-related BC components (BC^{FF} and BC^{BB}), while the ratios of the absorptions at different wavelengths follow a reciprocal power law of the wavelength ratio with a corresponding exponent (called Absorption Ångström Exponent, AAE) of FF- or BB-related BC. In this study, the source-specific AAE pair of 1.15 and 2.1 was used for the FF- and BB-related BC components respectively. The solution of the equation system results in the BB-related absorption at 950-nm wavelength whose ratio to the total absorption provides the ratio of the BB-related BC
190 concentration.

2.4.1 CO₂ source apportionment

In order to apply the carbon-balance method for the source-specific EF calculation, source apportionment of the carbon dioxide is needed as well, which was implemented using the BC source apportionment combined by multi-linear regression analysis (MLR). The method assumes that either the FF- or BB-related CO₂ component is correlated with the corresponding BC
195 component (BC^{FF} or BC^{BB}) in the plume. The total measured CO₂ can be expressed as follows:

$$CO_2(t) = CO_2^{FF}(t) + CO_2^{BB}(t) + CO_2^{bg}, \quad (2)$$

200 where $CO_2^{FF}(t)$ and $CO_2^{BB}(t)$ stand for the FF- and BB-related CO₂ components of the plume respectively, while CO_2^{bg} represents the background concentration that changes much slower than the combustion-related components; thus, it can be considered constant during a plume event.

Equation (2) can be formulated using the FF- and BB-related BC concentrations and emission ratios (ER^{FF} , ER^{BB}) as well:

$$CO_2(t) = \frac{BC^{FF}(t)}{ER^{FF}} + \frac{BC^{BB}(t)}{ER^{BB}} + CO_2^{bg}, \quad (3)$$

205

Or written in an equivalent form:

$$CO_2(t) = \frac{1}{ER^{FF}} \left[BC^{FF}(t) + \frac{ER^{FF}}{ER^{BB}} \cdot BC^{BB}(t) \right] + CO_2^{bg}, \quad (4)$$

210 Equation (4) expresses that the linear combination of $BC^{FF}(t)$ and $BC^{BB}(t)$ is correlated with the measured CO₂, using an appropriate ER^{FF}/ER^{BB} ratio. Our task is to find a particular ER^{FF}/ER^{BB} ratio, which provides the best correlation between the two sides of Eq. (4). After the best correlation was found, the slope of the regression line provides $1/ER^{FF}$, so ER^{BB} can be also calculated. The background CO₂ concentration determines the offset of the regression and is not needed to take into



consideration during the calculation. However, the background CO₂ provided by MLR is also a valuable information that we
215 are presenting in this paper.

The MLR analysis is a well-known and widely used method in source apportionment calculations; however, its combination
with the Aethalometer model just recently appeared in the literature. Kalogridis et al. (2018) used the source apportionment
information provided by the Aethalometer model for the source apportionment of carbon monoxide (CO) in Athens. They
compared their result with the linear CO-NO_x model (see there) and concluded that the CO-NO_x model overestimates the BB-
220 related CO contribution maybe due to the photochemical loss of NO_x, while the MLR analysis provided more reliable results.
The combination of the Aethalometer model with multi-linear regression analysis (AM-MLR) presented here thus can be a
universal technique for source apportionment of any air pollution component that emitted together with BC (for example CO₂,
CO, NO, NO₂, SO₂, PM or VOC).

For the application of the MLR analysis the R-statistical package (R Stats, Austria) was used. The correlations were studied in
225 a running time window with 1-hour duration. During this time interval the background concentration is supposed to be constant,
while the FF and BB sources have characteristic emission peaks.

It should be noted that during the 1-hour time window, several FF- and BB-related sources contribute to the measured plume
with different ERs. The emitted BC and CO₂ concentrations have been averaged out during the MLR, so the ER received from
the actual time window refers to the one hour average emission of the sources. The shorter the time window, the shorter the
230 averaging period, which results in higher variation and wider distribution of the ER values. However, the choice of the time
window does not affect the mode of the distribution (the most frequent ER value).

In the following special conditions, the MLR method provided false results, so they were discarded:

- 1) If the FF and BB components are well correlated ($R^2 > 0.8$) the MLR method cannot separate the two components and
provided similar ERs for the two components. Typically, this was the case when a transported pollution plume was
235 measured, within the FF and BB components arrived together to the measurement location resulting in correlated
concentration increments. In this case the ERs refer about the average BC emission ratio including all the combustion
sources (FF+BB) and must be discarded from the results.
- 2) Plumes dominated by one of the components results in good correlation between the BC component and the total CO₂
concentration. In this case the CO₂ source apportionment fails, and the total CO₂ increment is accounted for the
240 dominant source, consequently the calculation provides an underestimated EF. For this reason, cases when one of the
components correlated well with the total CO₂ concentration ($R^2 > 0.8$) were discarded from the analysis.
- 3) The maximal P-value for significance criteria was set to 10^{-5} for both components. Results exceeding this threshold
were discarded from the dataset.

2.5 Auxiliary measurements

245 For the validation of the AM-MLR method a well-defined case is needed with exclusively one type of sources (traffic or wood
burning). Since this was never the case during winter, we performed additional measurements during summertime next to the



E61 highway ring around Ljubljana, where the plumes were expected to originate from pure FF emission sources only. A portable monitoring unit was used for the measurement including an AE43 Aethalometer (Aerosol d.o.o, Slovenia) and a Vaisala GMP 343 CO₂ sensor, as in the winter campaign. The AE43 is a recently released battery-powered portable version of the AE33 Aethalometer with identical optical chamber, flow system and operation principle. In addition to its portable setup, the AE43 has a developed firmware and software system that offers improved user experiences with the real-time concentration, and pollution-rose plots.

The measurement station was installed on an overpass road above the highway. The overpass makes a connection between two sections of an unpaved road that has negligible traffic (mostly agricultural vehicles), so practically the highway emission dominates the concentrations. Due to the fast fluctuation of the concentration and the short lifetime of the pollution peaks emitted by individual sources, 1 second measurement time was used.

Since only FF-related sources were measured, the source apportionment and MLR procedures were not needed. The BC and the CO₂ concentration increments were well correlated during the peaks and the slope of the regression was considered as the ER^{FF}. Due to the rapid fluctuation of the concentrations, the regression was calculated using a 10-second running time window.

260 3 Results

3.1 Overview of the measurement results and diurnal cycle of the pollution

The statistical metrics of the hourly measurement averages at the three locations are summarised in Table 2. The BC^{FF} and BC^{BB} fractions are shown separately, as well as the CO₂ concentrations, temperature, and relative humidity. The meteorological parameters were measured at the BTC locations only but can be considered as generally valid values for the whole city area. It is seen that the traffic related BC^{FF} component dominates the BC load at all locations. The mean BC^{FF} concentrations were 2760, 2200, and 2650 ng m⁻³ at BTC, SKY and TRO locations, respectively; while the corresponding BC^{BB} concentrations were 1470, 1360, and 2180 ng m⁻³. The biggest difference between the FF- and BB-related components can be observed at BTC location (65% vs. 35% of total BC), while the smallest was at TRO (55% vs. 45%), indicating a higher influence of wood combustion in the historical centre of the city.

The spatial variation of the BC components shows an interesting pattern. Relative to the SKY location, the traffic-related FF component is higher by 26% at BTC and 20% at TRO. At the same time, the BB-related BC is higher by 8% at BTC; but 60% at TRO, indicating that this (TRO) location is a definite hotspot in terms of wood combustion. On the other hand, the influence of traffic emission from the surrounding busy roads is still significant at the TRO measurement site even though it is located in a restricted traffic area.

The daily variation of pollution can be followed in the composite day concentration plots shown in Figure 3. The FF- and BB-related BC concentrations are presented separately. It is seen that a pronounced FF peak can be found in the morning at 8:00 local time at all locations, representing traffic emissions during the morning rush hours.



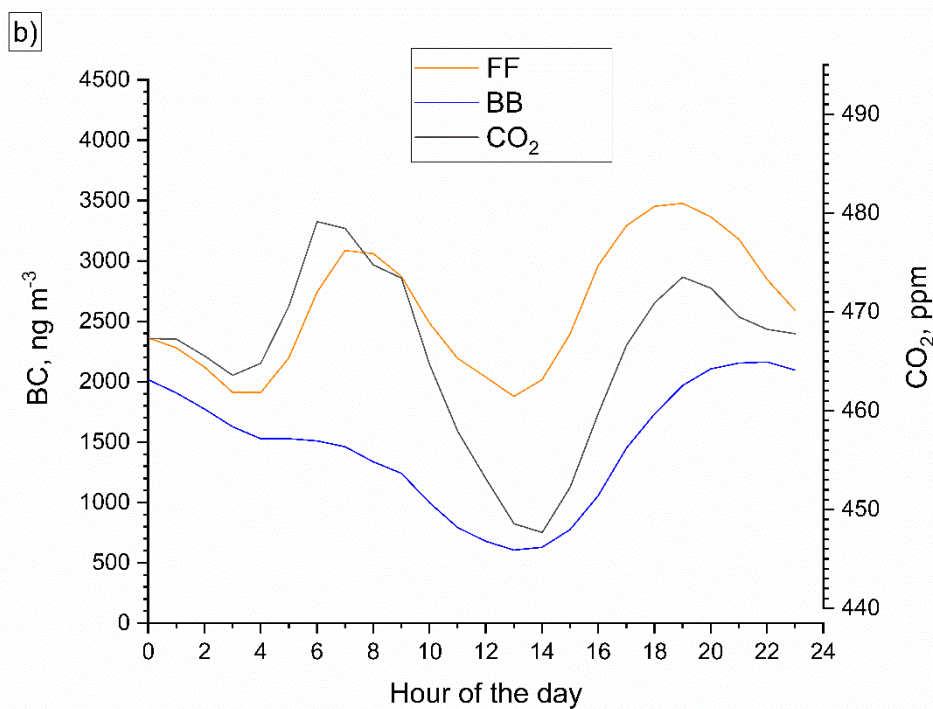
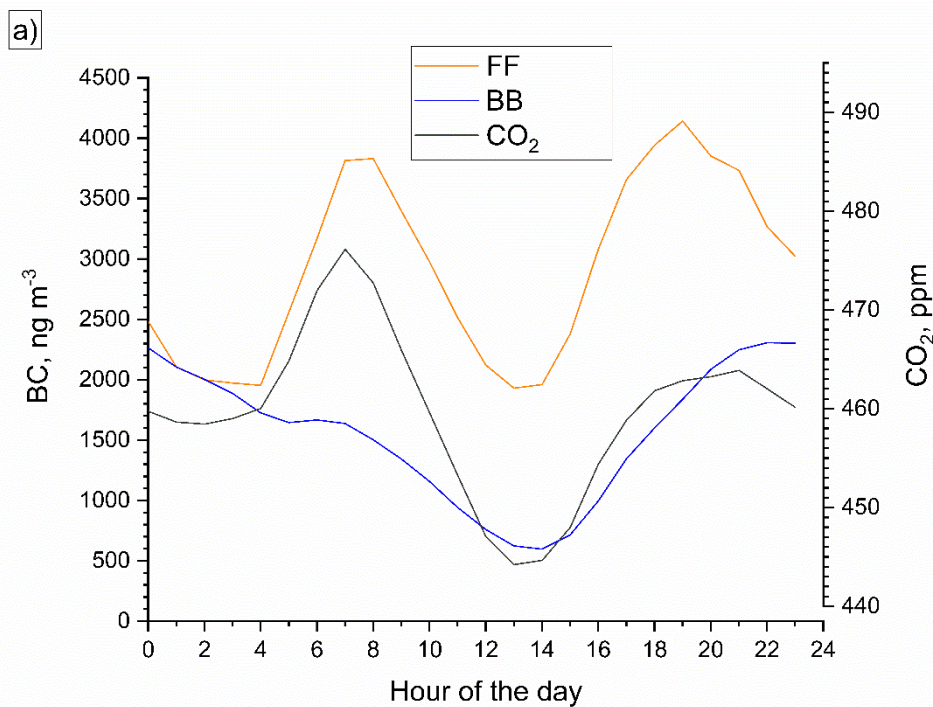
In contrary, the BB sources are more active in the afternoon. After 14:00 the BC^{BB} component starts to increase and reaches its daily maximum in the evening. An especially high evening maximum (3500 ng m^{-3}) was found at the BB-influenced TRO
280 location.

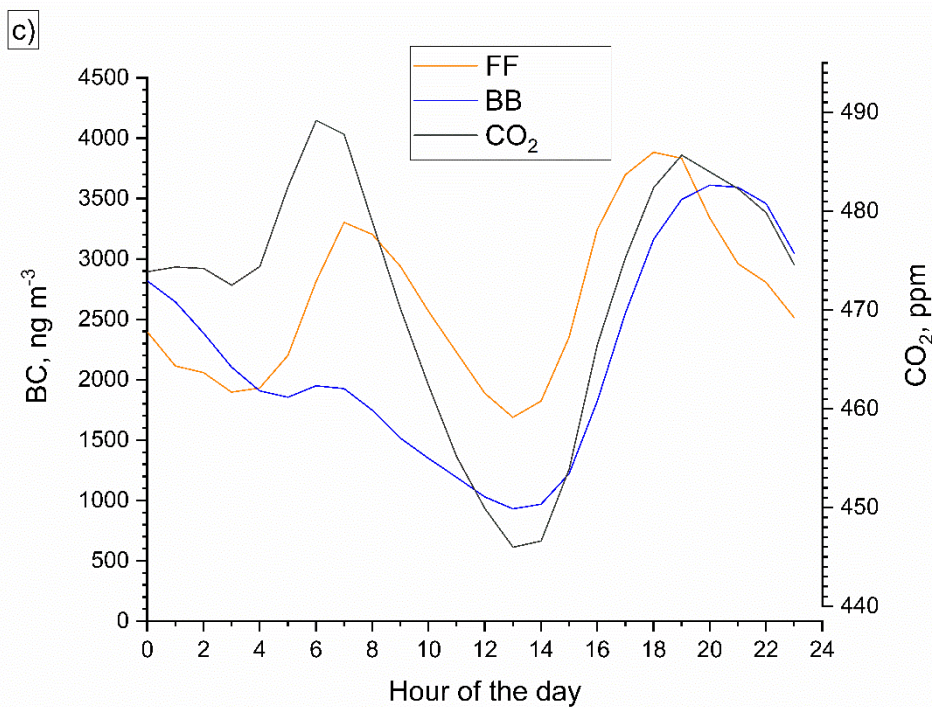


285 **BTC locations only.**

Table 2. Statistical metrics of the measurements at the three monitoring locations. Mean (with the source-specific percental share respecting the total BC), standard deviation (St. Dev.), their ratio (coefficient of variation, CV), the three quartiles (1Q, Median, 3Q), Minimum and Maximum values as well as their difference (Range) were calculated from hourly averages for the FF- and BB-related BC and CO₂ concentrations. Statistical values for the temperature (T) and relative humidity (RH) were given as well for the

	BC ^{FF} , ng m ⁻³			BC ^{BB} , ng m ⁻³			CO ₂ , ppm			T, °C	RH, %
	BTC	SKY	TRO	BTC	SKY	TRO	BTC	SKY	TRO	BTC	BTC
Mean	2760	2200	2650	1470	1360	2180	458	464	472	3.9	82.6
	65%	62%	55%	35%	38%	45%					
St. Dev.	2390	1990	2430	1510	1480	2350	29.4	33.3	43.9	5.2	15.1
CV	0.87	0.91	0.92	1.03	1.09	1.08	0.06	0.07	0.09	1.3	0.18
Min	30	40	50	10	20	10	407	411	406	-7.4	18.2
1Q	1023	749	903	292	219	397	434	436	434	-0.4	75.7
Median	2000	1540	1950	920	742	1280	454	458	462	4.0	88.7
3Q	3920	3030	3700	2230	2060	3200	476	485	497	8.2	94.1
Max	18900	16400	20700	8470	7450	14100	593	613	678	17.6	97.6
Range	18870	16360	20650	8460	7430	14090	186	202	272	25.0	79.4





290

Figure 3: Diurnal variation of the FF- and BB-related BC components as well as the CO₂ concentration at the a) BTC, b) SKY and c) TRO monitoring locations. The time scale represents local time.



3.2 BC/CO₂ emission ratios

295 Using the BC source apportionment results of the Aethalometer model, the MLR analysis provided the CO₂ source apportionment and the source-specific emission ratios. The normalised ER distributions are shown in Figure 4 for the three locations. The distributions are wide and follow a log-normal pattern, ranging from 10 to 1000 ng m⁻³/ppm according to the wide diversity of the sources. Log-normal curves were fitted on the distributions (solid lines in the figures), the parameters of which are summarised in Table 3. The mode and standard deviation that determines a normalised log-normal distribution are presented in the first two rows of the table. Since the median and mean differ from the mode for a log-normal distribution, these derived parameters are also shown in the last two rows of the table.

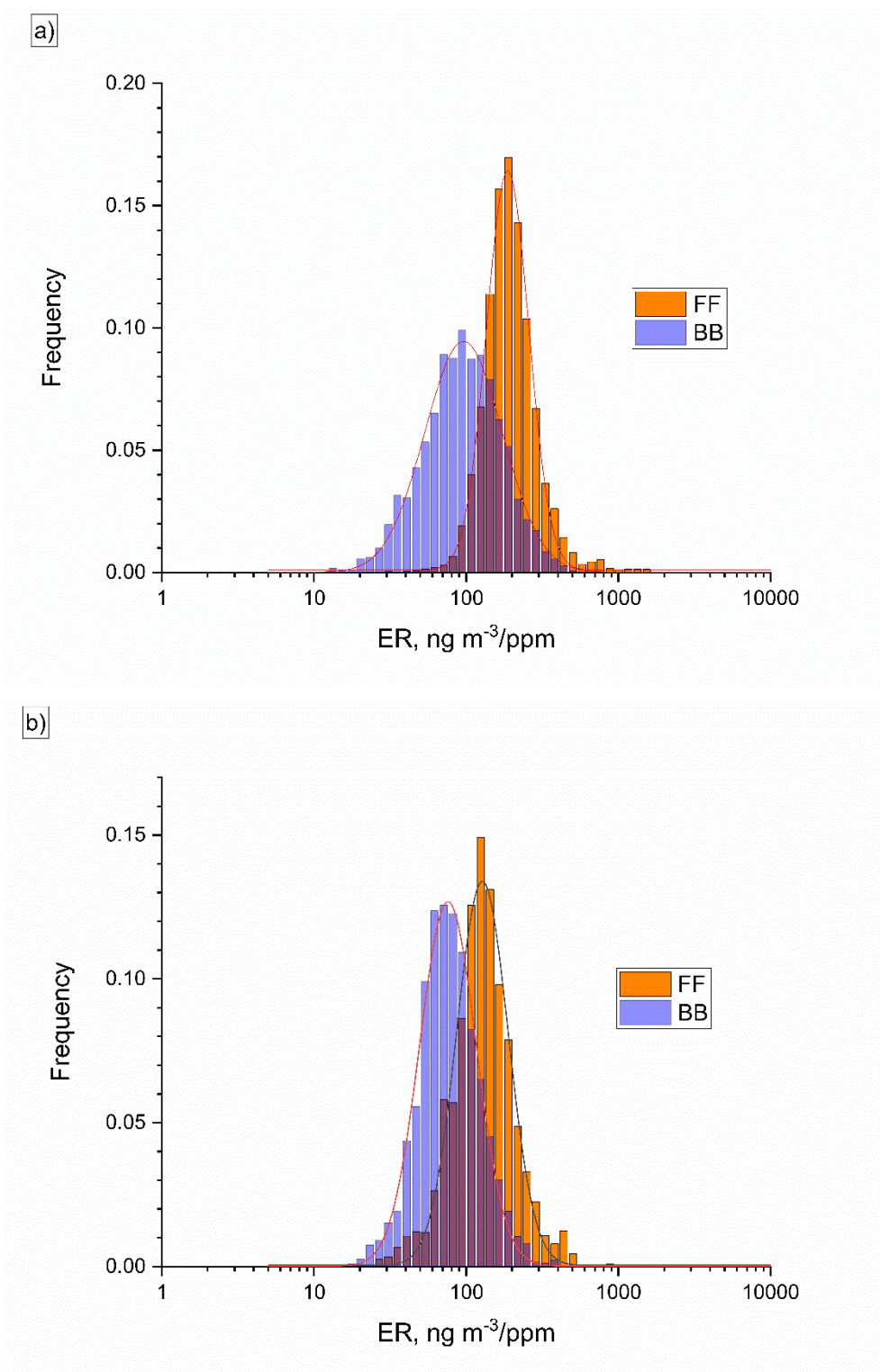
The wide distribution of ER can be explained by two main reasons. Firstly, the high variety of sources results in a wide range of emission ratios. For example, the BC emission factor of gasoline vehicles is in the range of 0.001-0.01 g (kg fuel)⁻¹, while that of diesel vehicles falls in 0.1-10 g (kg fuel)⁻¹ interval (EEA, 2019: 1.A.3.b.). Thus, the measured ER depends on the actual composition of the traffic, moving towards the higher values during the periods when the contribution of diesel sources (e.g. trucks, buses and goods vehicles) is higher. On the contrary, during periods when the traffic is dominated by personal vehicles, the ER decreases due to the higher contribution of gasoline vehicles.

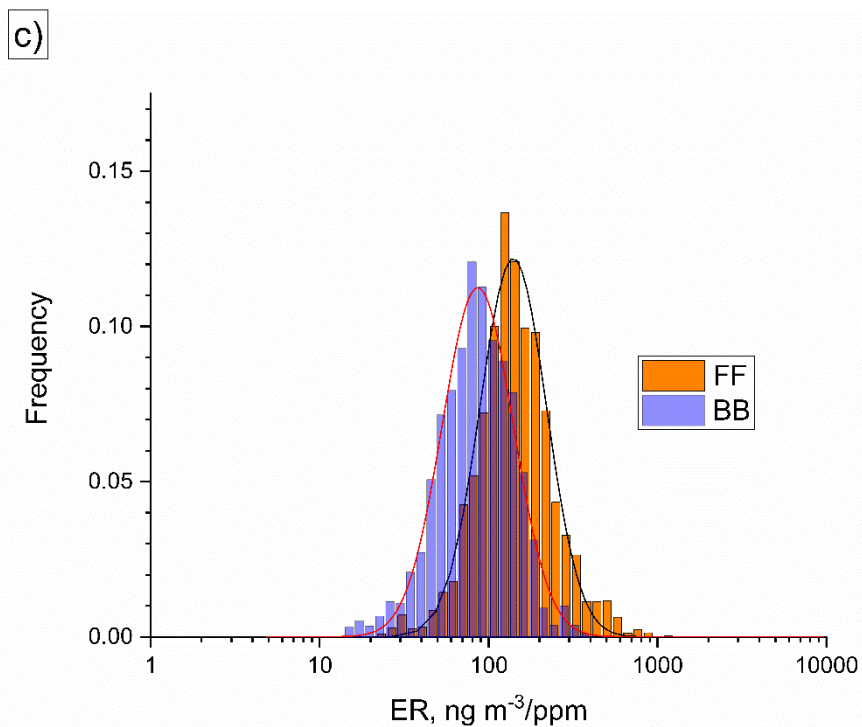
Regarding the BB sources, the contribution of gas heating to the combustion-related CO₂ emission must be taken into account. The BC emission of gas heaters is much smaller than that of wood burning (0.6 g/GJ vs. 74 g/GJ; EEA, 2019: 1.A.4.b), thus the contribution of gas burning in the CO₂ plume dilutes the BB-related emissions. At the same time, the different burning conditions of wood stows from smouldering to high temperature combustion, or the quality of the fuel (wood type, dryness degree) render high divergence of the emission ratios (see low fire – high fire variability in Table 6).

Additionally, the ER distribution widening may be the consequence of a measurement artefact caused by the high CO₂ background level. Typically, the combustion-related CO₂ increments were measured in the 8-55 ppm interquartile interval, while the average CO₂ background concentration was 437 ppm with 22 ppm interquartile range (see Table 7). This indicates how fast a combustion-related CO₂ increment can immerse in the fluctuation of the background during the dispersion of the plume. For this reason, sources with high ER (i.e., low CO₂ increment) can be detected close to the sources only, and their relative contribution decreases with increasing distance between the source and the measurement point. Therefore, diluted plumes always provide lower ERs than the direct ones, even if the composition of the sources is similar. Simultaneous measurement of direct and diluted plumes thus results in wider ER distribution with a lower mode compared to the direct measurement. The same phenomenon leads to lower ER values in well-mixed atmospheres, due to the dispersion of the CO₂ emission; while atmospheric inversion favours the detection of low CO₂ increments, thus resulting in higher ER.

Both the variation of the sources and the plume dispersion result in a typical diurnal pattern of the ER. Figure 5 shows the diurnal pattern of the (a) FF- and (b) BB-related ER at the BTC location as a typical example.

325





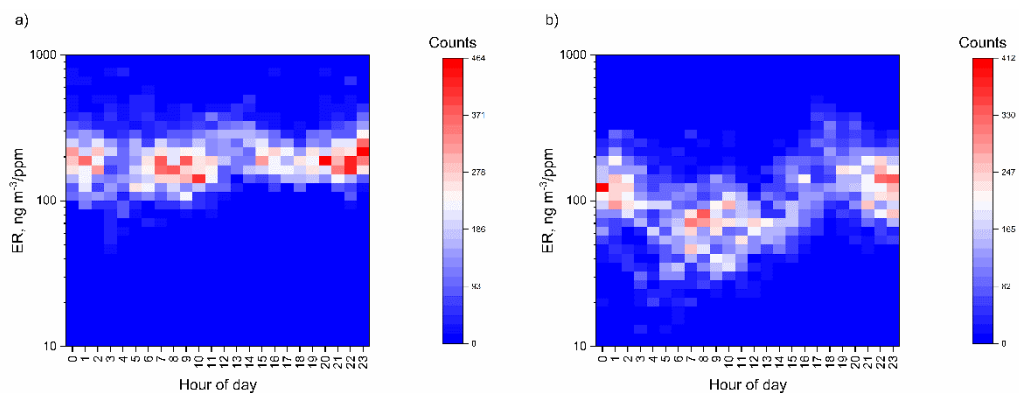
330 **Figure 4.** FF (orange) and BB (blue) related ERs at a) BTC, b) SKY and c) TRO locations respectively. The distributions are normalised to 1. Lognormal distributions (solid lines) were fitted to the results: the parameters are summarised in Table 3.



Table 3. Fitting parameters of the lognormal ER distributions ($\text{ng m}^{-3}/\text{ppm}$) at the three locations of the city. The distributions are normalised to 1. The derived Median and Mean ER values are also shown.

	BTC		SKY		TRO	
	FF	BB	FF	BB	FF	BB
Mode	187	96.1	128	75.8	140	88.5
St. Dev.	72.0	103	65.0	44.9	84.7	65.3
Median	208	136	149	91.2	169	112
Mean	219	161	160	100	185	126

335



340 **Figure 5. Diurnal variation of ER^{FF} (a) and ER^{BB} (b) distributions at BTC location (traffic site). Horizontal axes show the hour of the day while the ER is plotted on the vertical axes (logarithmic scale). The pixel colour corresponds to the number of counts in the ER bin.**

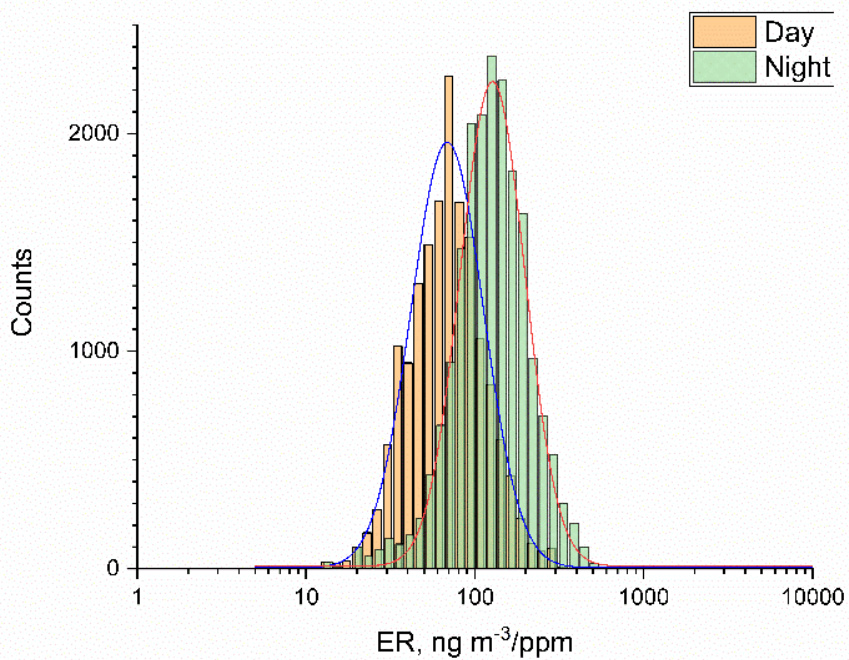


It is seen that ER^{FF} varies in a well-defined range between 100 and 300 $ng\ m^{-3}/ppm$ during the day, according to the direct
345 measurement of the sources (traffic site). On the other hand, ER^{BB} shows a clear diurnal pattern with a minimum during the
morning and maximum in the evening and night. The morning minimum can be attributed to the higher dilution of the pollution
due to atmospheric dynamics or higher relative contribution of gas burning, which shifts the ER distribution down according
to the above discussion. It can also be supposed that the combustion conditions are changing over the night from ignition
through flaming until smouldering phases that leads to different BC release relative to CO_2 emission. (For more detailed
350 relationship between combustion phases and emissions see Shen et al., 2021.)

Similar, but less pronounced diurnal pattern can be observed at the TRO location, while at the SKY location the ER^{BB}
distribution does not show significant daily variation (similarly to the ER^{FF} distribution at all the locations).

The wide distribution of the ER values at the BTC and TRO locations can be narrowed by data filtering based on the time.
Figure 6 shows biomass burning ER distributions measured at BTC location between 05:00 and 15:00 (Day) and 16:00-04:00
355 (Night) separately. Log-normal functions were fitted to the distributions, and the parameters are summarised in Table 4. The
same filtering was performed for the TRO location, while no filtering was applied for SKY location since the ER values did
not show a diurnal variation (parameters from Table 3 have been repeated).

After the time grouping, the daily ER values at the BTC and TRO locations got closer to each other and to the diurnal ER
value of the SKY location (68.7, 76.1, 75.8 $ng\ m^{-3}/ppm$ respectively). Since the SKY location is considered an urban
360 background location that is not directly affected by either traffic or biomass combustion, we can conclude that diluted and/or
transported plumes were measured at the BTC and TRO locations during the day-time period. On the other hand, significantly
higher ER values were measured during the night-time period (127 and 95.5 $ng\ m^{-3}/ppm$ at BTC and TRO, respectively) when
emissions of the nearby sources dominate the plume composition.



365

Figure 6. ER^{BB} distribution at the BTC location during daytime (05:00-15:00) and night-time (16:00-04:00) period. The lines show the fitted lognormal distributions (see parameters in Table 4).



370 **Table 4. Fitting parameters of the lognormal ER^{BB} distributions (ng m⁻³/ppm) measured at the BTC and TRO locations during day and night period. The distributions are normalised to 1. The derived Median and Mean are also presented. Values from Table 3 are repeated for the SKY location.**

	BTC		SKY	TRO	
	Day	Night		Day	Night
Mode	68.7	127	75.8	76.1	95.5
St. Dev.	52.3	79.3	44.9	62.9	61.3
Median	87.8	155	91.2	102	117
Mean	92.3	171	100	116	129



375 3.3 Emission factors of biomass burning and fossil fuel combustion

The emission factors were calculated from the ERs for biomass burning and traffic using Eq. (1). In Table 6 we show the results from our work together with other results of relevant studies from the literature. Mean values are shown in the table according to the literature data with the interquartile ranges in brackets.

We must note that the comparison of our results with the literature data is still problematic, for two main reasons. First, the
380 artefact caused by the high CO₂ background and diluted plume resulted in biased EFs that underestimate the real values. To minimize this bias, we present EFs where the effect of the dilution is most likely to be low (i.e. BTC measurement for FF and BTC & TRO night measurements for BB).

The second problem is that our results represent the average case of numerous urban sources involving low BC emitters (or non-smoking sources) that mostly contribute to the CO₂ increment (e.g. gas heating, gasoline vehicles). Thus, our results show
385 lower EFs than of individual sources published in the literature. In the following we discuss our results in the context of the literature data considering the above-mentioned aspects.

3.3.1 Traffic emission

The distribution of the traffic-related EF measured at BTC and at the highway is compared in Figure 7. Log-normal fits on the measured data are also shown. It is seen that the EF distribution at the highway site is much wider according to the applied
390 short averaging window (10 seconds) during MLR analysis that allows to detect even individual sources. On the other hand, the two distributions covering each other with similar modus (0.33 and 0.36 g/(kg fuel) at BTC and the highway respectively, see Table 5). This good agreement between the AM-MLR method and the pure FF measurement verifies the validity of the AM-MLR method and indicates that the EF values were not distorted by the dilution effect.

In Figure 7 relevant data from the literature are also shown in scatter plots (see more details in Table 6). Enroth et al. (2016)
395 studied EFs of a mixed fleet in Finland near a highway. Their mean EFs were in the 0.15-0.54 g/(kg fuel) range that overlaps with the EF distribution curve at BTC provided by the AM-MLR method (Fig. 7).

Blanco-Alegre et al. (2020) measured BC EF in a 1 km long urban tunnel in Braga, Portugal. Tunnels ensure well defined conditions for traffic EF measurements with concentrated pollution that mostly originates from vehicle emission. The authors obtained an average EF of 0.31 g/(kg fuel) for the fleet of nearly 56,000 vehicles, whose composition is probably similar to
400 the Slovenian fleet (Cooper, 2020). This value is in a very good agreement with the result of our AM-MLR method at BTC (0.39 g/(kg fuel) average).

Olivares et al. (2008) measured source-specific black carbon concentration in Temuco, Chile by Aethalometer and particle soot absorption photometer (PSAP). They determined the EF for mixed fleet by inverse modelling that gave results of 0.35 g/(kg fuel) mean EF for Aethalometer and 0.61-0.73 g/(kg fuel) EFs for PSAP that fit into our EF distribution.

405

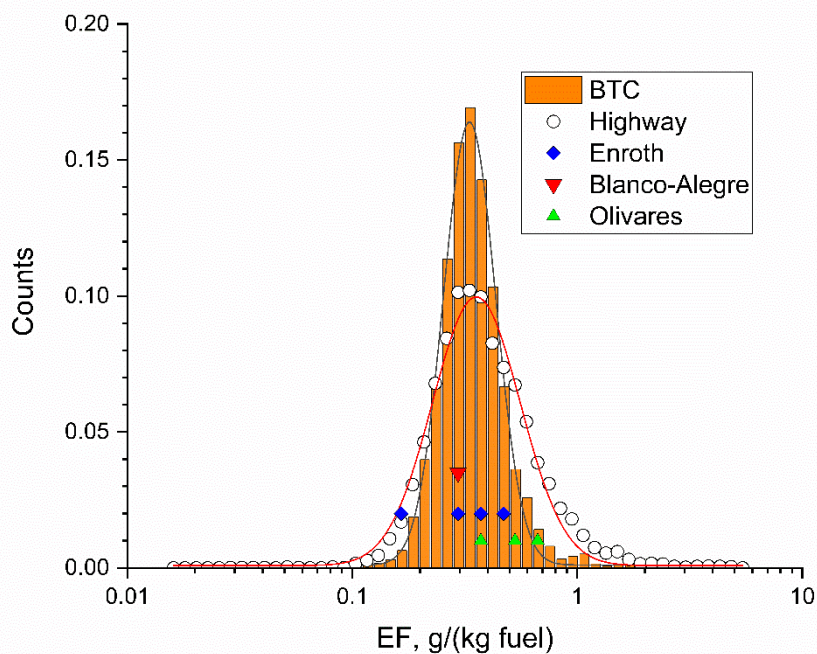


Figure 7. Distributions of the emission factors originated from traffic at BTC (bar chart) and the highway (scatter plot). Lognormal functions were fitted on the points with parameters summarised in Table 5. Coloured scatter symbols refer the literature data (only X-axes concerned). See more details in Table 6.

410



Table 5. Fitting parameters of the lognormal distributions of the fossil fuel related emission factor (EF, g/(kg fuel)) at BTC and the highway. The distributions are normalised to 1. The derived Median and Mean are also shown.

	BTC	Highway
Mode	0.33	0.36
St. Dev.	0.13	0.33
Median	0.37	0.49
Mean	0.39	0.56

415



Assuming that BC emissions of gasoline vehicles are negligible comparing to those of diesel engines (as is supported by tailpipe emission measurements – EEA 2019), all the measured BC^{FF} can be attributed to diesel emission. On the other hand, the diesel emission related carbon dioxide can be estimated based on the share of diesel cars in the vehicle fleet: namely, 36% in Slovenia (National interoperability framework – portal NIO, <https://nio.gov.si/nio>). This means that the diesel emission related CO_2 is roughly 36% of the total CO_2^{FF} . The emission factor of diesel engines thus can be calculated by dividing the original EF by 0.36.

In Table 6 the transformed EFs are presented for BTC and highway locations. These numbers refer the diesel EF only and they are in a good agreement with Brimblecombe et al. (2015), who reported 1.28 g/(kg fuel) diesel EF from a tunnel experiment in Hong Kong. The reported EF values from individual diesel cars (Ježek et al., 2015; Alves et al., 2015; Zavala et al., 2017; EEA, 2019) and individual truck emission monitoring (Ban-Weiss et al., 2009; Dallmann et al., 2011) are in a good agreement with our transformed EF distribution (Figure 8a).

3.3.2 Biomass burning

According to the literature data, the biomass burning EF from individual stove emission measurements ranges from 0.063 g/(kg fuel) (Sun et al., 2018) to 0.83 g/(kg fuel) (Holder et al. 2019; Akagi et al. 2011). The wide dispersion of the literature values indicates the high variety of BB EFs according to the stove type and combustion conditions. Figure 8b demonstrates that most of the literature EF data fall above our distribution measured at TRO location. The lower EFs we found here can be the consequences of the contribution of gas combustion sources that are common all around the city. Gas burning emits a very small mass of aerosol particles compared to wood combustion: but at the same time, it significantly contributes to the CO_2 emissions from domestic heating. Since gas combustion for heating probably has the same time pattern as wood combustion (i.e. concentration increments during the evening and cold weather, while drop during midday and warmer periods) the CO_2 increments that correlate with the BC^{BB} component partially originated from gas heating. Our method thus cannot uniquely identify EFs from pure wood combustion, but instead refers to the emission factor of the general domestic heating including non-smoking sources as well. In an ideal case, when the measured sources were exclusively fueled by wood, the heating-related EF would equal with the EF^{BB} , otherwise the higher the contribution of gas heating the lower the EF.

However, we also note that the real-world EF data published by Olivares et al. (2008) and the stove emission EF for pine tree by Sun et al. (2018) fall on the low end of the EF distribution measured at the TRO location.



445

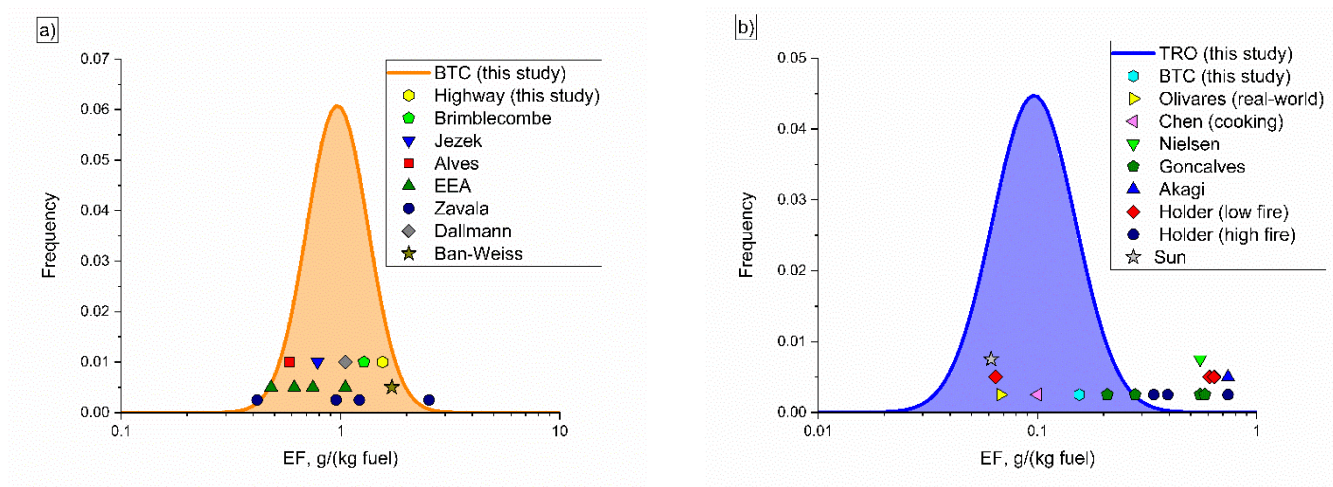


Figure 8. Distribution of the transformed FF EFs referring the diesel emission at the BTC location (a). Scatter points show the literature data and the highway measurement (only X-axis concerned). b) Distribution of the BB EFs at the TRO location. Scatter points show the literature data and the BTC result (only X-axis concerned). See more details in Table 6.

450



Table 6. Emission factors of fossil fuel and biomass burning sources. Comparison of the results of this study with the literature. Results from the present study are shown as mean values and interquartile range in brackets (q1-q3).

Source of data – measurement conditions	Emission factor, g/(kg fuel)	
	Fossil fuel (traffic)	Biomass burning
Enroth et al. (2016) highway study, 4 locations – mixed fleet	0.15; 0.30; 0.43; 0.54	
Blanco-Alegre <i>et al.</i> (2020), tunnel study – mixed fleet	0.31	
Brimblecombe <i>et al.</i> (2015), tunnel study – diesel fleet	1.28	
Ban-Weiss <i>et al.</i> (2009), tunnel study – individual diesel trucks	1.7	
Dallman <i>et al.</i> (2011), roadside study – individual diesel trucks	1.07	
Ježek <i>et al.</i> (2015), chasing measurement – individual diesel cars	0.79 (0.36-1.36)	
Zavala <i>et al.</i> (2017), chasing meas. – individual diesel vehicles	0.41; 0.94; 1.24; 2.48	
Alves <i>et al.</i> , 2015, dynamo chassis study – individual Euro4 and Euro3 diesel cars*	0.59; 0.58	
EEA (2019), dynamo chassis study – individual Euro4, Euro3, Euro2, Euro1 diesel cars respectively**	0.49; 0.62; 0.73; 1.02	
Olivares <i>et al.</i> (2008), street – mixed fleet , PSAP	0.61; 0.73	0.074
– mixed fleet , Aethalometer	0.35	
This study, highway – direct EF measurement	0.56 (0.28-0.59)	
Fleet apportionment corrected EF (36% diesel share)	1.57 (0.79-1.63)	
This study, BTC – AM-MLR source apportionment	0.39 (0.27-0.42)	0.16 (0.09 -0.17)
Fleet apportionment corrected EF (36% diesel share)	1.08 (0.75-1.16)	
This study, TRO – AM-MLR source apportionment		0.12 (0.07-0.13)
Akagi <i>et al.</i> (2011), open cooking		0.83
Chen <i>et al.</i> (2016), cooking		0.11
Nielsen <i>et al.</i> (2017), Nordic wood stove (9 kW), birch wood		0.62
Sun <i>et al.</i> (2018), pine tree		0.063
Goncalves <i>et al.</i> (2012), oak tree, pine tree – fireplace		0.30; 0.62
– traditional wood stove		0.23; 0.61
Holder <i>et al.</i> (2019), 3 different stoves, spruce wood – low fire		0.07; 0.68; 0.72
– high fire		0.37; 0.44; 0.83

*Converted from mg/km units using CO₂ EF from the same study.

455 **Converted from PM_{2.5} g/km EF using fuel consumption and BC percentage of PM_{2.5} published by the same study.



3.4 Source apportionment of CO₂ emission

Using the source apportionment of BC and the calculated BC ER values, the BB and FF source-related CO₂ components can
460 be retrieved. By subtracting the total combustion-related CO₂ increment from the measured CO₂ level, the non-combustion
related CO₂ level can be also determined.

Table 7 summarises the statistical metrics of the BB and FF source-related CO₂ concentrations as well as the background level
at the three measurement locations. In addition to the absolute mean values of the BB- and FF-related CO₂, their relative
contributions to the total combustion-related CO₂ concentration are also shown as percentiles.

465 It is seen that the average background CO₂ concentration was the same (~ 436 ppm) at all the locations. On the other hand, the
source apportionment of the combustion-related CO₂ shows significant variation according to the environmental conditions of
the locations. At the BTC location the FF-related CO₂ component is slightly lower than the BB component (47 vs. 53%), while
at the TRO location, the BB emission dominates the CO₂ level (62%).



470

Table 7. Source apportionment of the combustion-related CO₂ and the background level (Bg) at the three monitoring locations, as well as at the highway (FF component only). The Mean (with the percental share respecting the total combustion-related CO₂), standard deviation (St. Dev.), their ratio (coefficient of variation, CV), the three quartiles (1Q, Median, 3Q), Minimum and Maximum values as well as their difference (Range) were calculated from hourly averages for the FF- and BB-related CO₂

475 **concentration increments.**

CO ₂ , ppm	BTC			SKY			TRO			HW	
	FF	BB	Bg	FF	BB	Bg	FF	BB	Bg	FF	Bg
Mean	19.9 47%	22.4 53%	437	21.8 44%	27.7 56%	435	25.9 38%	41.9 62%	437	34.5 100%	498
Stl. Dev.	16.1	16.4	11.2	17.2	18.7	9.67	20.8	28.5	16.9	18.1	22.6
CV	0.80	0.73	0.02	0.79	0.68	0.02	0.80	0.68	0.04	0.52	0.04
Min	2.67	3.54	422	2.30	6.2	424	2.68	8.19	418	2.67	440
1Q	8.29	9.89	428	9.63	13.9	428	11.9	20.6	424	21.7	482
Median	15.7	18.7	434	17.1	22.8	433	20.2	35.2	433	31.5	493
3Q	26.4	30.2	443	29.0	36.2	439	33.3	55.7	446	43.5	512
Max	148	171	492	130	159	496	143	198	511	286	587
Range	146	167	70.0	128	153	72.0	140	190	94.2	284	147



4 Conclusions

480 Atmospheric concentrations of black carbon and CO₂ were monitored real-time at three urban locations in Ljubljana, Slovenia that had different impacts of traffic and wood-burning during the winter heating season. The source-specific BC concentrations from the Aethalometer model were used to apportion the combustion-related CO₂ by coupling a multi-linear regression method. The analysis presumed two combustion-related sources, namely domestic heating (biomass burning) and traffic (fossil fuel combustion). The combined AM-MLR method provided consistent and realistic “real-world” emission ratios and emission factors for the three measurement locations. The method can be further generalised for source apportionment of other
485 combustion-related components that of EFs can be later determined. Information about the source specific EFs helps to estimate the pollution emission based on the fuel consumption.

The specific conclusions are the follows:

1. The traffic-related BC^{FF} concentration was higher than BC^{BB} at all locations. The smallest difference was found at TRO (wood combustion site), while the largest difference was obtained at BTC (traffic site). In contrast, the heating related CO₂ concentration were higher at all locations.
490
2. The determined ERs follow a wide log-normal distribution according to the variety of the fuels (from the non-smoking gasoline or natural gas to the BC producing diesel oil and wood) and sources (DPF equipped vs. conventional diesel vehicles; different types and conditions of wood stoves), as well as combustion conditions (high temperature, excess of air vs. low temperature, deficit air conditions). Also, it was shown that the distances of the sources affect the ER, since the relative contribution of high ER sources (means low relative CO₂ emission) are lower for higher distances due to the dilution of the related CO₂ increment.
495
3. Using the literature data of the carbon content of the fuels (diesel oil vs. wood) the related emission factors (EF) were determined. The determined mean traffic-related EF (0.39 g/(kg fuel)) is in a good agreement with published EF values for a mixed traffic fleet. Using the relative ratio of gasoline and diesel fleet for Slovenia, the diesel emission related EF could be calculated (1.08 g/(kg fuel)) that is in good agreement with diesel emission factors published in the literature.
500
4. The BB-related mean EF (0.16 g/(kg fuel)) is lower than the majority of the relevant literature data values reported for individual stoves. This is due to the CO₂ contribution of other, non-smoking combustion sources (i.e. gas heating).
5. The AM-MLR method was validated by direct traffic emission monitoring next to the highway during summertime, when only traffic-related sources were most likely sampled. Thus, the FF-related emission factors could be directly
505 determined without source apportionment. The similarity of the modes of the two distributions indicates that the AM-MLR method provided reliable results.



Data availability

510 Data presented in the paper are available at the authors upon request.

Authors contribution

AG and IJ designed the experiments with the supervision and guidance of MR; while BA, MI and AG carried out the measurements. BA developed the methodology for CO₂ source apportionment and EF calculations. AG performed the MLR analysis by the R-statistical software package. BA prepared the manuscript with contributions from all co-authors.

515 Competing interests

At the time of the research, the authors were employed by the manufacturer of the Aethalometer instruments, used to measure black carbon concentration in the study. The funding sponsors had no role in the design of the study; in the collection, analyses, or interpretation of data; in the writing of the manuscript; or in the decision to publish the results.

Acknowledgements

520 This research was funded by the Ministry of Economic Development and Technology of Slovenia (grant number: C2130-19-096947) and the Slovenian Research Agency (J1-1716 D). Antony Hansen is thanked for his comments and corrections that helped to finalise the manuscript.

References

- 525 Akagi, S. K., Yokelson, R. J., Wiedinmyer, C., Alvarado, M. J., Reid, J. S., Karl, T., Crounse, J. D., and Wennberg, P.O.: Emission factors for open and domestic biomass burning for use in atmospheric models, *Atmos. Chem. Phys.*, 11, 4039–4072, doi:10.5194/acp-11-4039-2011, 2011.
- Alves, C. A., Lopes, D. J., Calvo, A. I., Evtyugina, M., Rocha, S., Nunes, T.: Emissions from Light-Duty Diesel and Gasoline in-use Vehicles Measured on Chassis Dynamometer Test Cycles, *Aerosol and Air Quality Research*, 15, 99–116, doi: 10.4209/aaqr.2014.01.0006, 2015.
- 530 Ban-Weiss, G. A., Lunden, M. M., Kirchstetter, T. W., Harley, R. A.: Measurement of black carbon and particle number emission factors from individual heavy-duty trucks, *Environmental Science and Technology*, 43, 1419–1424, 2009, doi: 10.1021/es8021039.
- Blanco-Alegre, C., Calvo, A. I., Alves, C., Fialho, P., Nunes, T., Gomes, J., Castro, A., Oduber F., Coz, E., Fraile, R.: Aethalometer measurements in a road tunnel: A step forward in the characterization of black carbon emissions from



- 535 traffic, *Science of the Total Environment*, 703, 135483, 2020.
- Bond, T. C., & Bergstrom, R. W.: Light Absorption by Carbonaceous Particles: An Investigative Review, *Aerosol Sci. and Technol.*, 40, 27–67, doi: 10.1080/02786820500421521, 2006.
- Brimblecombe, P., Townsend, T., Lau, C. F., Rakowska, A., Chan, T. L., Mocnik, G., Ning, Z.: Through-tunnel estimates of vehicle fleet emission factors, *Atmospheric Environment*, 123, 180-189, 2015.
- 540 Brown, S. G., Lam-Snyder, J., McCarthy, M. C., Pavlovic, N. R., D'Andrea, S., Hanson, J., Sullivan, A. P., Hafner, H. R.: Assessment of Ambient Air Toxics and Wood Smoke Pollution among Communities in Sacramento County. *Int. J. Environ. Res. Public Health.*, 17(3), 1080, doi: 10.3390/ijerph17031080, 2020.
- Chen, Y., Shen, G., Liu, W., Du, W., Su, S., Duan, Y., Lin, N., Zhuo, S., Wang, X., Xing, B., Tao, S.: Field measurement and estimate of gaseous and particle pollutant emissions from cooking and space heating processes in rural households, northern China, *Atmospheric Environment*, 125, 265-271, 2016.
- 545 Chen, J., Li, C., Ristovski, Z., Milic, A., Gu, Y., Islam, M.S., Wang, S., Hao, J., Zhang, H., He, C., Guo, H., Fu, H., Miljevic, B., Morawska, L., Thai, P., Fat LAM, Y., Pereira, G., Ding, A., Huang, X., Dumka, U.C.: A review of biomass burning: Emissions and impacts on air quality, health and climate in China, *Science of The Total Environment*, 579, 1000-1034, doi:10.1016/j.scitotenv.2016.11.025, 2017.
- 550 Chiloane, K. E., Beukes, J. P., van Zyl, P. G., Maritz, P., Vakkari, V., Josipovic, M., Venter, A. D., Jaars, K., Tiitta, P., Kulmala, M., Wiedensohler, A., Liousse, C., Mkhathshwa, G. V., Ramandh, A., and Laakso, L.: Spatial, temporal and source contribution assessments of black carbon over the northern interior of South Africa, *Atmos. Chem. Phys.*, 17, 6177–6196, doi:10.5194/acp-17-6177-2017, 2017.
- Cooper, J. (edit): Statistical Report 2020, *Fuels Europe*, www.fuelseurope.eu/wp-content/uploads/SR_FuelsEurope-_2020-1.pdf, 2020.
- 555 Cuesta-Mosquera, A., Močnik, G., Drinovec, L., Müller, T., Pfeifer, S., Cruz Minguillón, M., Briel, B., Buckley, P., Dudoitis, V., Fernández-García, J., Fernández-Amado, M., Ferreira De Brito, J., Riffault, V., Flentje, H., Heffernan, E., Kalivitis, N., Kalogridis, A. C., Keernik, H., Marmureanu, L., Luoma, K., Marinoni, A., Pikridas, M., Schauer, G., Serfozo, N., Servomaa, H., Titos, G., Yus-Díez, J., Ziola, N., and Wiedensohler A.: Intercomparison and characterization of 23 Aethalometers under laboratory and ambient air conditions: procedures and unit-to-unit variabilities, *Atmos. Meas. Tech.*, 14, 3195–3216, doi:10.5194/amt-14-3195-2021, 2021.
- 560 Dallmann, T. R., Harley, R. A., and Kirchstetter, T. W.: Effects of diesel particle filter retrofits and accelerated fleet turnover on drayage truck emissions at the port of Oakland, *Environmental Science and Technology*, 45, 10773-10779, 2011, doi: 10.1021/es202609q.
- 565 Deng, J., Guo, H., Zhang, H., Zhu, J., Wang, X., and Fu, P.: Source apportionment of black carbon aerosols from light absorption observation and source-oriented modeling: an implication in a coastal city in China, *Atmos. Chem. Phys.*, 20, 14419–14435, doi:10.5194/acp-20-14419-2020, 2020.



- Drinovec, L., Mocnik, G., Zotter, P., Prevot, A. S. H., Ruckstuhl, C., Coz, E., Rupakheti, M., Sciare, J., Müller, T., Wiedensohler, and Hansen, A. D. A.: The "dual-spot" Aethalometer: An improved measurement of aerosol black carbon with real-time loading compensation, *Atmos. Meas. Tech.*, 8, 1965-1979, 2015.
- 570 Dumka, U. C., Kaskaoutis, D. G., Tiwari, S., Safai, P. D., Attri, S. D., Soni, V. K., Singh, N., Mihalopoulos, N.: Assessment of biomass burning and fossil fuel contribution to black carbon concentrations in Delhi during winter, *Atmos. Environ.*, 194, 93-109, doi:10.1016/j.atmosenv.2018.09.033, 2018.
- EEA: EMEP/EEA air pollution emission inventory guidebook. Technical guidance to prepare national emission inventories, EEA Report No 13/2019, ISSN 1977-8449, doi:10.2800/293657, 2019.
- 575 Enroth, J., Saarikoski, S., Niemi, J., Kousa, A., Ježek, I., Mocnik G., Carbone, S., Kuuluvainen, H., Rönkkö, T., Hillamo, R., and Pirjola, L.: Chemical and physical characterization of traffic particles in four different highway environments in the Helsinki metropolitan area, *Atmos. Chem. Phys.* 16, 5497-5512, doi:10.5194/acp-16-5497-2016, 2016.
- Giechaskiel, B., Bonnel, P., Perujo, A., Dilara, P.: Solid Particle Number (SPN) Portable Emissions Measurement Systems (PEMS) in the European Legislation: A Review. *International Journal of Environmental Research and Public Health.* 16(23), 4819, doi:10.3390/ijerph16234819, 2019.
- 580 Giglio, L., Randerson, J. T., van der Werf, G. R.: Analysis of daily, monthly, and annual burned area using the fourth-generation global fire emissions database (GFED4), *J. Geophys. Res. Biogeosci.*, 118, 317-328, doi:10.1002/jgrg.20042, 2013.
- 585 Glojek, K., Močnik, G., Alas, H. D. C., Cuesta-Mosquera, A., Drinovec, L., Gregorič, A., Ogrin, M., Weinhold, K., Ježek, I., Müller, T., Rigler, M., Remškar, M., van Pinxteren, D., Herrmann, H., Ristorini, M., Merkel, M., Markelj, M., and Wiedensohler, A.: The impact of temperature inversions on black carbon and particle mass concentrations in a mountainous area, *Atmos. Chem. Phys. Discuss.* [preprint], doi:10.5194/acp-2021-869, in review, 2021.
- Gonçalves, C., Alves, C., Pio, C.: Inventory of fine particulate organic compound emissions from residential wood combustion in Portugal, *Atmospheric Environment*, 50, 297-306, doi:10.1016/j.atmosenv.2011.12.013, 2012.
- 590 Hansen, A. D. A., and Rosen, H.: Individual measurement of the emission factor of aerosol black carbon in automobile plumes, *J. Air Waste Manage. Assoc.*, 40, 1654-1657, 1990.
- Healy, R. M., Wang, J. M., Sofowote, U., Su, Y., Deboz, J., Noble, M., Munoz, A., Jeong, C-H., Hilker, N., Evans, G. J., Doerksen G.: Black carbon in the Lower Fraser Valley, British Columbia: Impact of 2017 wildfires on local air quality and aerosol optical properties, *Atmospheric Environment*, 217, 116976, doi:10.1016/j.atmosenv.2019.116976, 2019.
- 595 Helin, A., Niemi, J. V., Virkkula, A., Pirjola, L., Teinila, K., Backman, J., Aurela, M., Saarikoski, S., Ronkko, T., Asmi, E., and Timonen, H.: Characteristics and source apportionment of black carbon in the Helsinki metropolitan area, Finland, *Atmos. Environ.*, 190, 87-98, 2018.
- Holder, A. L., Yelverton, T. L. B., Brashear, A. T., Kariher, P. H.: Black carbon emissions from residential wood combustion appliances, US-EPA report, EPA/600/R-20/039, May, 2019.
- 600



- Huss, A., Maas, H., and Hass, H.: Well-to-wheels analysis of future automotive fuels and powertrains in the European context, Tankto-wheels (TTW) report, version 4, EC Joint Research Centre, Luxembourg, doi:10.2788/40409, 2013.
- Janssen, N. A. H., Hoek, G., Simic-Lawson, M., Fischer, P., van Bree, L., ten Brink, H., Keuken, M., Atkinson, R. W., Anderson, H. R., Brunekreef, B., Cassee, F. R.: Black carbon as an additional indicator of the adverse health effects of Airborne particles compared with PM₁₀ and PM_{2.5}, *Environ. Health Perspect.* 119 (12), 1691–1699. doi:10.1289/ehp.1003369, 2011.
- Ježek, I., Katrasnik, T., Westerdahl, D., and Mocnik, G.: Black carbon, particle number concentration and nitrogen oxide emission factors of random in-use vehicles measured with the on-road chasing method, *Atmospheric Chemistry and Physics*, 15, 11011–2015, doi:10.5194/acp-15-11011-2015, 2015.
- Kalogridis, A. C., Vratolis, S., Liakakou, E., Gerasopoulos, E., Mihalopoulos, N., and Eleftheriadis, K.: Assessment of wood burning versus fossil fuel contribution to wintertime black carbon and carbon monoxide concentrations in Athens, Greece, *Atmos. Chem. Phys.*, 18, 10219–10236, doi:10.5194/acp-18-10219-2018, 2018, 2018.
- Karagulian, F., Belis, C. A., Dora, C. F. C., Prüss-Ustün, A. M., Bonjour, S., Adair-Rohani, H., Amann, M.: Contributions to cities' ambient particulate matter (PM): A systematic review of local source contributions at global level, *Atmos. Env.*, 120, 475–483, 2015.
- Karanasiou, A., Alastuey, A., Amato, F., Renzi, M., Stafoggia, M., Tobias, A., Reche, C., Forastiere, F., Gumy, S., Mudu, P., Querol, X.: Short-term health effects from outdoor exposure to biomass burning emissions: A review, *Science of The Total Environment*, 781, 146739, doi:10.1016/j.scitotenv.2021.146739, 2021.
- Klimont, Z., Kupiainen, K., Heyes, C., Purohit, P., Cofala, J., Rafaj, P., Borcken-Kleefeld, J., and Schöpp, W.: Global anthropogenic emissions of particulate matter including black carbon, *Atmos. Chem. Phys.*, 17, 8681–8723, doi:10.5194/acp-17-8681-2017, 2017.
- Liakakou, E., Stavroulas, I., Kaskaoutis, D. G., Grivas, G., Paraskevopoulou, D., Dumka, U. C., Tsagkaraki, M., Bougiatioti, A., Oikonomou, K., Sciare, J., Gerasopoulos, E., Mihalopoulos, N.: Long-term variability, source apportionment and spectral properties of black carbon at an urban background site in Athens, Greece, *Atmos. Env.*, 222, 117137, doi:10.1016/j.atmosenv.2019.117137, 2020.
- Mbengue, S., Serfozo, N., Schwarz, J., Zikova, N., Smejkalova, A. H.: Holoubek, I.: Characterization of Equivalent Black Carbon at a Regional Background Site in Central Europe: Variability and Source Apportionment, *Environ. Pollut.*, 260, 113771, 2020.
- Milinković, A., Gregorič, A., Džaja Grgičin, V., Vidič, S., Penezić, A., Cvitešić Kušan, A., Bakija Alempijević, S., Kasper-Giebl, A., Frka, S.: Variability of black carbon aerosol concentrations and sources at a Mediterranean coastal region, *Atmospheric Pollution Research*, 12 (11), doi:10.1016/j.apr.2021.101221, 2021.
- Mitchell, E. J. S., Coulson, G., Butt, E. W., Forster, P. M., Jones, J. M., Williams, A.: Heating with biomass in the United Kingdom: Lessons from New Zealand, *Atmospheric Environment*, 152, 431–454, doi:10.1016/j.atmosenv.2016.12.042, 2017.



- 635 Myhre, G., Samset B. H., Schulz, M., Balkanski, Y., Bauer, S., Berntsen T. K., Bian, H., Bellouin, N., Chin, M., Diehl, T.,
Easter R. C., Feichter, J., Ghan, S. J., Hauglustaine, D., Iversen T., Kinne, S., Kirkevag, A., Lamarque, J. F., Lin, G.,
Liu, X., Lund, M. T., Luo, G., Ma, X., van Noije, T., Penner, J. E., Rasch, P. J., Ruiz, A., Seland, Ø., Skeie, R. B.,
Stier, P., Takemura, T., Tsigaridis, K., Wang, P., Wang, Z., Xu, L., Yu, H., Yu, F., Yoon, J. H., Zhang, K., Zhang,
H., and Zhou, C.: Radiative forcing of the direct aerosol effect from AeroCom Phase II simulations, *Atmos. Chem.*
640 *Phys.*, 13, 7683-7693, 2013.
- Naeher, L. P., Brauer, M., Lipsett, M., Zelikoff, J. T., Simpson, C. D., Koenig, J. Q., Smith, K. R.: Woodsmoke Health Effects:
A Review, *Inhalation Toxicol.*, 19 (1), 67–106, 2007.
- Nielsen, I. E., Eriksson, A. C., Lindgren, R., Martinsson, J., Nystrom, R., Nordin, E. Z., Sadiktsis, I., Boman, C., Nøjgaard, J.
K., Pagels, J.: Time-resolved analysis of particle emissions from residential biomass combustion – Emissions of
645 refractory black carbon, PAHs and organic tracers, *Atmospheric Environment*, 165, 179-190, 2017.
- Olivares, G., Ström, J., Johansson, C., Gidhagen, L.: Estimates of black carbon and size-resolved particle number emission
factors from residential wood burning based on ambient monitoring and model simulations, *Journal of the Air &
Waste Management Association*, 58 (6), 838-848, doi: 10.3155/1047-3289.58.6.838, 2008.
- Park, G., Kim, K., Park, T., Kang, S., Ban, J., Choi, S., Yu, D. G., Lee, S., Lim, Y., Kim, S., Lee, J., Woo, J. H., and Lee, T.:
650 Characterizing black carbon emissions from gasoline, LPG, and diesel vehicles via transient chassis-dynamometer
tests, *Appl. Sci.*, 10, 5856, doi:10.3390/app10175856, 2020.
- Querol, X. (project coordinator): Emission Factors of Biomass Burning, Life-AIRUSE report 9, LIFE11/ENV/ES/584,
2016/12, 2016.
- Reddington, C. L., Morgan, W. T., Darbyshire, E., Brito, J., Coe, H., Artaxo, P., Scott, C. E., Marsham, J., and Spracklen,
655 D.V.: Biomass burning aerosol over the Amazon: analysis of aircraft, surface and satellite observations using a global
aerosol model, *Atmos. Chem. Phys.*, 19, 9125–9152, doi:10.5194/acp-19-9125-2019, 2019, 2019.
- Sánchez-Ccoyllo, O. R., Ynoue, R. Y., Martins, L. D., Astolfo, R., Miranda, R. M., Freitas, E. D., Borges, A. S., Fornaro, A.,
Freitas, H., Moreira, A., Andrade, M.F.: Vehicular particulate matter emissions in road tunnels in Sao Paulo, Brazil,
Environmental Monitoring and Assessment, 149 (1), 241-249, doi:10.1007/s10661-008-0198-5, 2009.
- 660 Sandradewi, J., Prevot, A. S. H., Szidat, S., Perron, N., Alfarra, R. M., Lanz, V. A., Weingarten, E., and Baltensperger, U.:
Using aerosol light absorption measurements for the quantitative determination of wood burning and traffic emission
contributions to particulate matter, *Environ. Sci. Technol.*, 42, 3316-3323, 2008.
- Shen, H., Luo, Z., Xiong, R., Liu, X., Zhang, L., Li, Y., Du, W., Chen, Y., Cheng, H., Shen, G., Tao, S.: A critical review of
pollutant emission from fuel combustion in home stoves, *Environment International*, 157, 106841, 2021, doi:
665 10.1016/j.envint.2021.106841.
- Sigsgaard, T., Forsberg, B., Annesi-Maesano, I., Blomberg, A., Bølling, A., Boman, C., Bønløkke, J., Brauer, M., Bruce, N.,
Héroux, M. E., Hirvonen, M. R., Kelly, F., Künzli, N., Lundbäck, B., Moshhammer, H., Noonan, C., Pagels, J.,



- Sallsten, G., Sculier, J. P., Brunekreef, B.: Health Impacts of Anthropogenic Biomass Burning in the Developed World, *Eur. Respir. J.*, 46 (6), 1577–1588, 2015.
- 670 Smirnov, N. S., Korotkov, V. N., and Romanovskaya, A. A.: Black carbon emission from wildfires on forest lands of the Russian Federation 2007-2017, *Russ. Meteorol. Hydrol.*, 40, 435–442, doi:10.3103/S1068373915070018, 2015.
- Sun, J., Zhi, G., Jin, W., Chen, Y., Shen, G., Tian, C., Zhang, Y., Zong, Z., Cheng, M., Zhang, X., Zhang, Y., Liu, C., Lu, J., Wang, H., Xiang, J., Tong, L., Zhang, X.: Emission factors of organic carbon and elemental carbon for residential coal and biomass fuels in China- A new database for 39 fuel-stove combinations, *Atmos. Env.*, 190, 241-248, doi:10.1016/j.atmosenv.2018.07.032, 2018.
- 675 Tomlin, A. S.: Air Quality and Climate Impacts of Biomass Use as an Energy Source: A Review *Energy & Fuels*, 35 (18), 14213-14240, doi:10.1021/acs.energyfuels.1c01523, 2021.
- Trubetskaya, A., Lin, C., Ovadnevaite, J., Ceburnis, D., O’Dowd, C., Leahy, J. J., Monaghan, R. F. D., Johnson, R., Layden, P., and Smith, W.: Study of Emissions from Domestic Solid-Fuel Stove Combustion in Ireland, *Energy & Fuels*, 35 (6), 4966-4978, doi: 10.1021/acs.energyfuels.0c04148, 2021.
- 680 Val Martin, M., Honrath, R. E., Owen, R. C., Pfister, G., Fialho, P., and Barata F.: Significant enhancements of nitrogen oxides, black carbon, and ozone in the North Atlantic lower free troposphere resulting from North American boreal wildfires, *J. Geophys. Res.*, 111, D23S60, doi:10.1029/2006JD007530, 2006.
- Wang, X., Westerdahl, D., Hu, J., Wu, Y., Yin, H., Pan, X., Zhang, K.M.: On-road diesel vehicle emission factors for nitrogen oxides and black carbon in two Chinese cities, *Atmospheric Environment*, 46, 45-55, 2012.
- 685 Weingartner, E., Saathoff, H., Schnaiter, M., Streit, N., Bitnar, B., Baltensperger, U.: Absorption of light by soot particles: determination of the absorption coefficient by means of aethalometers, *Journal of Aerosol Science*, 34 (10), 1445-1463, doi:10.1016/S0021-8502(03)00359-8, 2003.
- Zavala, M., Molina, L. T., Yacovitch, T. I., Fortner, E.C., Roscioli, J. R., Floerchinger, C., Herndon, S. C., Kolb, C. E., Knighton, W. B., Paramo, V. H., Zirath, S., Mejía, J. A., and Jazcilevich, A.: Emission factors of black carbon and co-pollutants from diesel vehicles in Mexico City, *Atmos. Chem. Phys.*, 17, 15293–15305, doi:10.5194/acp-17-15293-2017, 2017.
- 690 Zheng, X., Wu, Y., Jiang, J., Zhang, S., Liu, H., Song, S., Li, Z., Fan, X., Fu, L., and Hao, J.: Characteristics of On-road Diesel Vehicles: Black Carbon Emissions in Chinese Cities Based on Portable Emissions Measurement, *Environmental Science & Technology*, 49 (22), 13492-13500, doi:10.1021/acs.est.5b04129, 2015.
- 695